Reliability of inserts in sandwich composite panels

Bryan Smith*, Biswajit Banerjee*

Industrial Research Limited
24 Balfour Road, Parnell
Auckland 1052, New Zealand

Abstract

Inserts are commonly used to transfer loads to sandwich composite structures. Local stress concentrations due to inserts are known to cause structural failure, and experimental pull-out tests show that the failure load can vary by 20% between batches of sandwich panels. Clearly, uncertainty in the mechanical properties of the constituent materials needs to be addressed in the design and optimization of sandwich panel inserts. In this paper, we explore the utility of reliability analysis in design, applying Monte Carlo sampling, the first order reliability method (FORM), line sampling, and subset simulation to a one-dimensional model of an insert in a homogenized sandwich panel. We observe that for systems with very low failure probabilities, subset simulation is the most efficient method for calculating the probability of structural failure, but in general, Monte Carlo sampling is more effective than the advanced reliability analysis techniques.

Keywords: Statistical Methods, Computational Modelling, Stress Concentrations, Strength

*Corresponding author.
Email addresses: bryan.smith@irl.cri.nz (Bryan Smith), b.banerjee@irl.cri.nz (Biswajit Banerjee)

1. Introduction

Sandwich composite panels are used widely in the aerospace and marine industries, and various configurations of inserts are employed to join panels together and to attach external objects [1]. Figure 1 shows an example schematic of an insert. The insert is attached by an adhesive potting compound to a panel consisting of two facesheets and a honeycomb or foam core [2]. While the insert shown in the figure is blind, through the thickness inserts are also common.

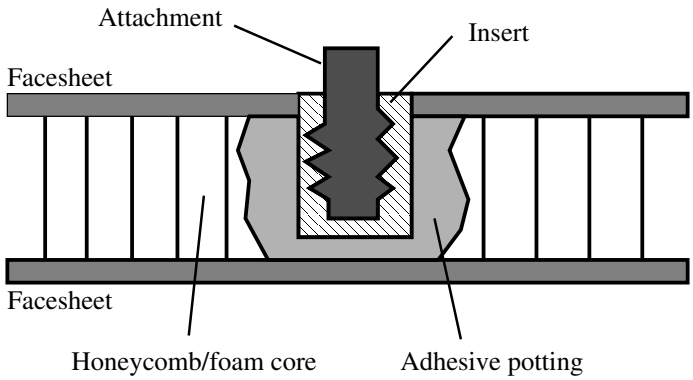

Figure 1: An insert in a sandwich panel.

Inserts act both as localized regions of load application and as stress concentrators [3, 4, 5], and therefore the performance of a sandwich panel is quite sensitive to variations in the material, geometry, and load in the region of the insert [6, 7, 8]. In this paper we explore the use of several reliability analysis techniques to characterize the relationship between the applied load and the probability of structural failure in the presence of parametric uncertainty. In industrial applications, the panel and the insert may be subjected to various types of loads, but here we only consider a load normal to the plane of the panel. Several studies [3, 9, 10] suggest that under these loading conditions, the initial failure event is a debond of the pot-

ting from the core, followed by buckling of the honeycomb and fracture/yield of the facesheets. However, we are unaware of any studies addressing reliability of these structures in the presence of material and geometric variability.

For simplicity and efficiency, we use a one-dimensional axisymmetric model [11] of a sandwich panel in our study. The structure consists of four components: two facesheets, a honeycomb core, and the adhesive potting. It is important to note that though the honeycomb buckles under small loads, the effect of this buckling is not obvious in load-displacement curves from pull-out tests and three-point bend tests [1, 10]. Thus, a single criterion for localized failure is an insufficient indicator of macroscopic failure. Since macroscopic failure is of most interest to design engineers, we consider two multi-component failure criteria. In the first situation, system failure is assumed to have occurred when *any two* of the structural components satisfy certain failure criteria, and in the second situation, failure occurs when *any three* components fail.

Sources of uncertainty in the sandwich-insert model include the geometry, the material properties, and the applied loads. A distinction could possibly be made between inherent variability (or aleatoric uncertainty) and reducible uncertainty (or epistemic uncertainty) [12], but for the purpose of this study, all uncertainty is assumed to be due to inherent variability. In the event of improvement in our knowledge of the materials or loads, that new knowledge will change only the expected values and probability distributions that we used to characterize the variability in our reliability analysis. We ignore detailed micromechanical causes of variability and focus only on the macroscopically observable statistics. Normal distributions with assumed standard deviations are used for parameters for which sufficient data are not available.

The simplest method for calculating the probability of failure is Monte Carlo sampling. However, this method is inefficient for situations with low failure probabilities, so several methods, including the First-order reliability method (FORM) [13], line sampling [14], and subset simulation [15] have been developed to reduce the computational cost of determining low probabilities of failure. The principal finding of our work is that for problems with a complex failure sequence and multiple failure regions within the parameter space, subset simulation is the most efficient method for determining the structural reliability at low failure probabilities. However, for failure probabilities of the order typically dealt with by composite designers, none of the advanced reliability analysis methods demonstrate a clear advantage over Monte Carlo sampling.

The paper is organized as follows. In Section 2, we describe the one-dimensional axisymmetric model of a sandwich panel with an insert. Comparisons of the theory with one- and two-dimensional finite element simulations are provided. Reliability theory and various approaches for uncertainty propagation are briefly explained in Section 3. In Section 4, finite element simulations are used to determine the estimated reliability of sandwich composites with inserts for various levels of parameter variability. The results are discussed and conclusions drawn in Section 5.

2. Modeling sandwich panels with inserts

The numerical simulation of sandwich structures containing inserts can be computationally expensive. This is particularly true when the goal is a statistical analysis of the effect of variable input parameters on the response of the structure. Simplified theories of sandwich structures provide an efficient means of reliabil-

ity analysis under these circumstances. Models of sandwich structures can be broadly classified into the following types:

- Single- and multi-layer layer models that do not account for changes in thickness. Such models include first-order linear models [16], higher-order linear models [17], and geometrically-exact nonlinear models [18].

- Single- and multi-layer models that do account for thickness changes. These include linear single-layer models [19, 20, 21], nonlinear single-layer models [22, 23, 24, 25, 26], and linear multi-layer models [11, 27, 28, 29, 30].

Single-layer models attempt to model the mechanics of sandwich panels in a manner similar to beam and plate theory by adding extra degrees of freedom to a single reference surface. Additional effects due to the presence of inserts are difficult to incorporate into such models. Multi-layer models are more convenient when modeling inserts in sandwich panels. Also, changes in panel thickness become important when potted inserts are subjected to pull-out loads. Hence, the linear theory of sandwich panels with inserts proposed by Thomsen et al. [11, 27, 28] appears to be appropriate for a reliability analysis of sandwich panels with inserts. It should be noted that local nonlinear effects (both material and geometric) close to an insert become pronounced as the deformation proceeds. However, in the interest of simplicity, we ignore nonlinear effects in this work.

2.1. The Thomsen model

In the original version of the Thomsen model, plate theory was used to develop three sets of governing equations (for the two facesheets and the core). These equations were coupled through traction and displacement boundary conditions at the interfaces between the facesheets and the core. The resulting system of

first order ordinary differential equations was solved by Thomsen using a multi-segment finite-difference method. The insert was assumed to be rigid and the potting around the insert was modeled as a core material. The model was designed so that both normal and shear pull-out loads could be applied to the insert.

In our work, we have applied the Thomsen approach to an axisymmetric sandwich panel with a through-the-thickness insert. Instead of Thomsen's numerical method, we have used a considerably simpler finite element approach to discretize and solve the governing system of ordinary differential equations.

A schematic of an axisymmetric sandwich panel is shown in Figure 2. The panel has a radius r_a and consists of two facesheets and a core. An adhesive potting of radius r_p is used to bond a rigid insert of radius r_i to the panel. A vertical force is applied to the insert in the positive z-direction. A clamp is attached to the panel at a distance r_c from the center to prevent rigid-body motions due to the applied force. The core thickness is $2c$, the top facesheet thickness is $2f^{\text{top}}$, and the thickness of the bottom facesheet is $2f^{\text{bot}}$. The extensional and bending stiffnesses of the facesheets are $A_{ij} = 2fC_{ij}$ and $D_{ij} = 2f^3/3C_{ij}$, where C_{ij} $(i, j = 1, 2)$ are components of the stiffness matrix relating the stresses $\sigma_{rr}, \sigma_{\theta\theta}$ to the strains $\varepsilon_{rr}, \varepsilon_{\theta\theta}$. For the core, the transverse stiffness (C_{33}) is defined by the relation $\sigma_{zz} = C_{33}\varepsilon_{zz}$ while the shear *compliance* (S_{55}) is defined by $\varepsilon_{rz} = S_{55}\sigma_{rz}$. The potting is assumed to have the same behavior as the core, i.e., it is characterized by the two material constants, C_{33} and S_{55}.

A detailed derivation of the equations governing the deformation of the panel (and their weak forms) can be found elsewhere [31]. A summary of the relevant equations is given below. Conservation of linear and angular momentum in the facesheets can be expressed as two equations, one for the balance of stress resul-

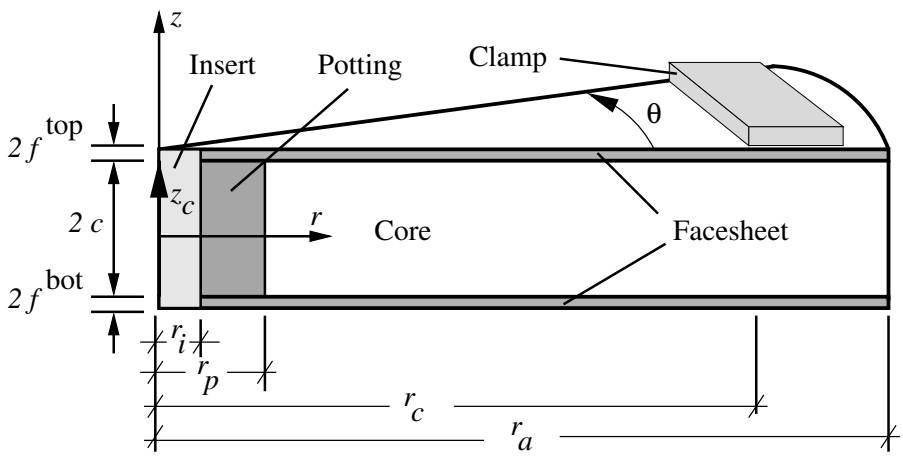

Figure 2: The geometry of an axisymmetric sandwich panel with insert and potting.

tants and the other for the balance of stress moment resultants. The balance of stress resultants in the *top facesheet* leads to the weak form

$$\int_{\Omega_0} \left[N_{rr}^{\text{top}} \frac{d\delta u_{0r}^{\text{top}}}{dr} + \left\{ \frac{N_{\theta\theta}^{\text{top}}}{r} + \sigma_{rz}^{\text{core}} - s^{\text{tt}} \right\} \delta u_{0r}^{\text{top}} \right] d\Omega_0 = \oint_{\Gamma_0} N_r^{\text{top}} \delta u_{0r}^{\text{top}} d\Gamma_0 \,. \qquad (1)$$

A similar equation can be found for the bottom facesheet. The mid-surface of the facesheet is assumed to be the reference surface for all calculations in this paper.

In the above equation Ω_0 is the two-dimensional reference surface of the facesheet, Γ_0 is its one-dimensional boundary, u_{0r} is the radial displacement of points on the reference surface, $N_{rr}, N_{\theta\theta}$ are the radial and circumferential stress resultants in the facesheets, and N_r is a boundary force term. The quantity N_r is, of course, distinct from N_{rr}. A surface traction (at the top of the top facesheet) s^{tt} has also been included in the equation to allow for possible shear loads. The stress resultants are given by

$$N_{rr} = A_{11}\, u_{0r,r} + A_{12}\, u_{0r}/r \;; \;\; N_{\theta\theta} = A_{12}\, u_{0r,r} + A_{11}\, u_{0r}/r,$$

where A_{ij} are the extensional stiffnesses of the facesheet. Observe *the core shear*

stress term (σ_{rz}) in equation (1. From the point of view of the facesheets, this is the term that couples the facesheets to the core.

A balance of stress moment resultants in the top facesheet can be expressed as

$$\int_{\Omega_0} \left[M_{rr}^{\text{top}} \frac{d^2 \delta w_0^{\text{top}}}{dr^2} + \left\{ \frac{M_{\theta\theta}^{\text{top}}}{r} - f^{\text{top}} \left(s^{\text{tt}} - \sigma_{rz}^{\text{core}} \right) \right\} \frac{d\delta w_0^{\text{top}}}{dr} \right.$$
$$\left. - \left\{ \frac{C_{33}^{\text{core}}}{2c} (w_0^{\text{top}} - w_0^{\text{bot}}) - c \frac{d\sigma_{rz}^{\text{core}}}{dr} - c \frac{\sigma_{rz}^{\text{core}}}{r} \right\} \delta w_0^{\text{top}} \right] d\Omega_0$$
$$= \oint_{\Gamma_0} \left[M_r^{\text{top}} \frac{d\delta w_0^{\text{top}}}{dr} - Q_z^{\text{top}} \delta w_0^{\text{top}} \right] d\Gamma_0. \quad (2)$$

A similar equation can be found for the bottom facesheet. In the above equation w_0 is the z-direction displacement of the mid-surface of the facesheet and stress moment resultants are given by:

$$M_{rr} = -D_{11}\, w_{0,rr} - D_{12}\, w_{0,r}/r \;; \;\; M_{\theta\theta} = -D_{12}\, w_{0,rr} - D_{11}\, w_{0,r}/r,$$

where D_{ij} are the bending stiffnesses, M_r is a bending moment, and Q_z is a shear force.

Notice that equation (2) contains another coupling term w_0^{bot} in addition to $\sigma_{rz}^{\text{core}}$ which indicates that this equation is couple both to the core and to the bottom facesheet. Equations (1) and (2) have counterparts when we consider the bottom facesheets and these four coupled equations describe the deformation of the facesheets. We now need an equation that describes the deformation of the core.

Equilibrium of the core in the presence of the two facesheets requires that the

core shear stress satisfies the equation,

$$\int_{\Omega_0}\left[\frac{d\sigma_{rz}^{\text{core}}}{dr}\frac{d\delta\sigma_{rz}}{dr}+\frac{1}{r}\left(\sigma_{rz}^{\text{core}}\frac{d\delta\sigma_{rz}}{dr}+\frac{d\sigma_{rz}^{\text{core}}}{dr}\delta\sigma_{rz}\right)+\left\{\left(\frac{1}{r^2}+\frac{6C_{33}^{\text{core}}S_{55}^{\text{core}}}{c^2}\right)\sigma_{rz}^{\text{core}}\right.\right.$$
$$\left.\left.-\frac{3C_{33}^{\text{core}}}{2c^3}\left[u_{0r}^{\text{top}}-u_{0r}^{\text{bot}}+\left(f^{\text{top}}+c\right)\frac{dw_0^{\text{top}}}{dr}+\left(f^{\text{bot}}+c\right)\frac{dw_0^{\text{bot}}}{dr}\right]\right\}\delta\sigma_{rz}\right]d\Omega_0$$
$$=\oint_{\Gamma_0}\left(\frac{d\sigma_{rz}^{\text{core}}}{dr}+\frac{\sigma_{rz}^{\text{core}}}{r}\right)\delta\sigma_{rz}d\Gamma_0. \quad (3)$$

The core shear stress is therefore coupled to the facesheet deformations via the variables u_{0r} and w_0. Therefore we have a system of five coupled equations, (*equations* (1) *and* (2) *for both facesheets, and equation* (3) *for the core*), which can be discretized using finite elements. We have solved these equations with the finite element code Comsol®. Quadratic shape functions have been used for the u-displacement and σ-stress, and cubic Hermite functions for the w-displacement.

2.2. The insert pull-out test

To simulate a pull-out test, a vertical shear traction is applied to the inner surface of the potting while u_r at that location is constrained to zero. The shear stress, σ_{rz}, is set to zero at the free end of the panel, and the points at which the panel is clamped are constrained such that $w_0 = 0$. Stability of the solution requires that both the top and the bottom facesheets be clamped. The potting is modelled as a core with properties that are derived from those of the actual potting material. Note that the potting, like the core, is assumed to have no extensional stiffness in the plane of the sandwich panel. There is a discontinuity in material properties at the potting radius (r_p), but no special boundary conditions are required for a through insert when the appropriate elements are used. For a part-through (or

potted) insert, special conditions on the displacements are required (for details see [31]). However, we only consider through thickness inserts.

To verify that the one-dimensional model produces reasonable results, it has been compared with a two-dimensional axisymmetric model simulated with the Abaqus® finite element code. Figure 3 shows that the one-dimensional model provides a reasonable estimate of the core shear stress but underestimates the displacement (compared with the two-dimensional model). The sandwich panel geometry and material properties for these calculations can be found in [10]. The stresses in the facesheets are overestimated while those in the potting are underestimated by the one-dimensional model and, partly due to the small displacements and the linear nature of the model, the potting is never observed to fail in our simulations. However, we ignore these issues in this work and focus on the computation of reliability.

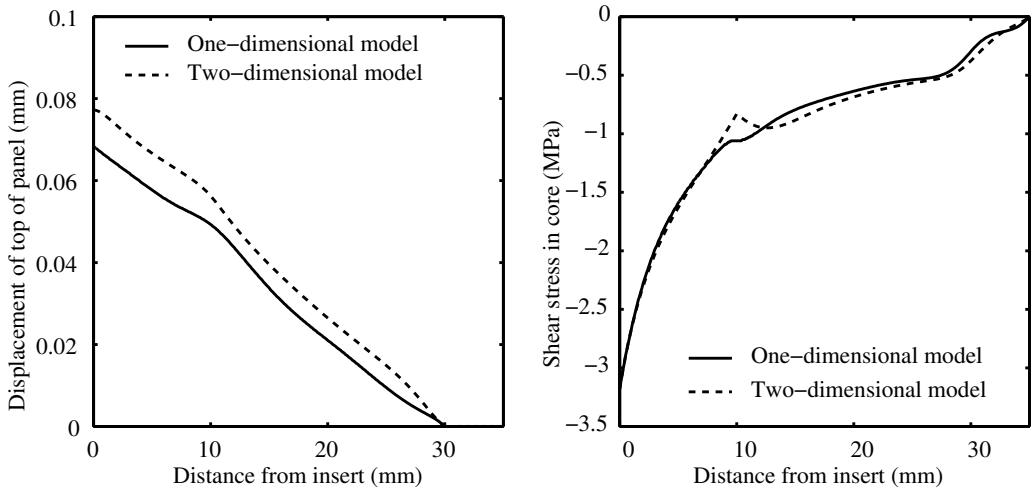

Figure 3: Comparisons between one-dimensional (solid) and two-dimensional models (dotted).

2.3. System failure

The reliability estimates that we seek require the determination of a global failure surface for the model. There are four components in the structure that can fail at different loads; the two facesheets, the core, and the potting. One could take the failure load to be the smallest load at which any of these components fail. In fact, simulations of detailed honeycomb sandwich panels under pull-out loads show that the core buckles at relatively small loads (see Figure 4 for an example of localized buckling at loads less than 1 kN). But load-deflection curves from the same simulations do not indicate any deviation from linearity at these loads, let alone failure. Therefore, a global failure surface constructed on the basis of the "first component to fail" may not be ideal for reliability analyses of sandwich composites.

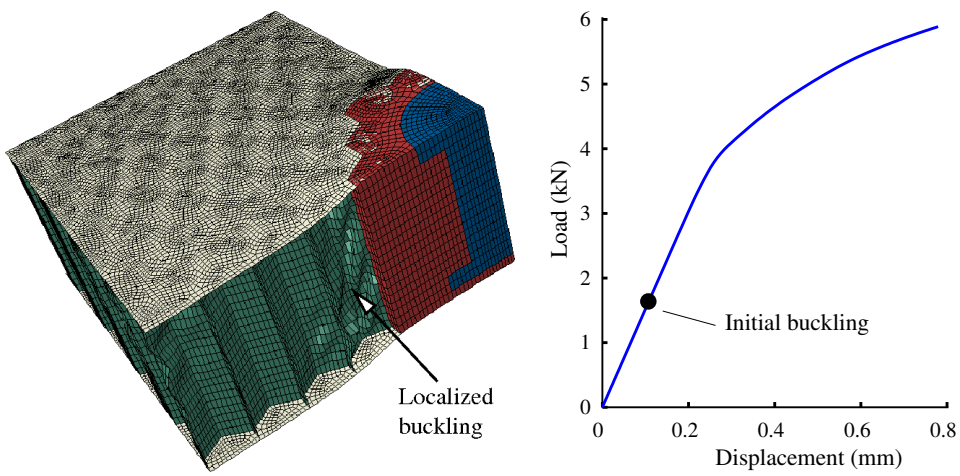

Figure 4: Localized buckling of the core in an aluminum honeycomb sandwich panel with an insert under pull-out load.

The procedure that we use to populate the global failure surface is as follows. A pull-out load is applied to the one-dimensional finite element model. The core

and potting stresses (σ_{rz}, σ_{zz}) and the facesheet stresses ($\sigma_{rr}, \sigma_{\theta\theta}$) are computed at each element. The stress in each of these elements is identified and fed into the failure criterion appropriate for the component to which the element belongs.

In this study, von Mises failure criteria (Tsai-Wu criterion with isotropic properties) have been used for the aluminum facesheets and the potting. The yield stresses for these materials have been obtained from [10]. Compressive (buckling) and shear failure stresses in the aluminum honeycomb have been calculated using the formulae in Gibson and Ashby ([32], p. 171). A quadratic core collapse criterion that uses the compressive and shear stresses in the core has been used to flag failure of the honeycomb [33].

The global failure surface is *not populated* if we observe failure in *only one* component. If more than one component appears to have failed, we explore two options. The first option is designated "*two-component failure*" and the structure is assumed to have failed when at least two failure criteria have been exceeded. The second option is designated "*three-component failure*". In this case, the failure of at least three components is sought before we populate the failure surface. This approach leads to performance functions that do not necessarily have a high degree of smoothness and is useful for examining the strengths and weaknesses of various techniques of reliability analysis.

3. Reliability Analysis

A reliability analysis determines the relationship between the model parameters, $\boldsymbol{\theta}$, a d-dimensional vector with known input probability distributions, and p_f, the probability of structural failure. If $g(\boldsymbol{\theta})$ is a C^0 continuous *performance function* constructed such that $g(\boldsymbol{\theta}) \leq 0$ when $\boldsymbol{\theta}$ lies in the failure domain and

$g(\boldsymbol{\theta}) > 0$ in the safe domain, p_f can be defined as:

$$p_f = \int_{g(\boldsymbol{\theta}) \leq 0} h(\boldsymbol{\theta})\, d\boldsymbol{\theta} = \int_{\mathbb{R}^d} \mathbf{1}_F(\boldsymbol{\theta})\, h(\boldsymbol{\theta})\, d\boldsymbol{\theta}, \tag{4}$$

where $h(\boldsymbol{\theta})$ is the joint probability density function of the parameters and $\mathbf{1}_F(\boldsymbol{\theta})$ is an indicator function (equal to one in the failure region and zero elsewhere). For independent and identically distributed (i.i.d.) parameters, the joint probability density function can be calculated using

$$h(\boldsymbol{\theta}) = \prod_{i=1}^{d} \phi(\theta_i), \quad \text{with} \quad \phi(\theta) = \frac{1}{\sqrt{2\pi}}\, e^{-\theta^2/2} \tag{5}$$

where ϕ is the *standard normal probability density function* (p.d.f.). Correlated variables can be converted into an independent set using classical techniques such as the Nataf transformation. Also, parameters that are not identically distributed can be usually be transformed and normalized. Therefore, conversion of a non i.i.d set of parameters into a set that satisfies equation (5) simplifies the analysis considerably. However, the performance function $g(\boldsymbol{\theta})$ is rarely known explicitly and typically must be evaluated at individual points in the design space.

The simplest and most reliable method for computing p_f is *Monte Carlo sampling* (MCS) in which N realisations of $\boldsymbol{\theta}$ are generated and an estimator, $\bar{p}_f = \frac{1}{N}\sum_{i=1}^{N} \mathbf{1}_F(\boldsymbol{\theta}_i)$, for the failure probability is computed. If the samples are drawn from the full domain of parameter space, the expression for the coefficient of variation (CoV) of the Monte Carlo estimator is given by $\delta_{\mathrm{MC}} = \sqrt{(1-p_f)/(p_f N)}$. This expression indicates that in order to achieve a 10% CoV, approximately $100/p_f$ samples must be evaluated. Multiple performance function evaluations are computationally expensive, so a variety of techniques have been developed to minimize the required number of simulations.

The *First Order Reliability Method* (FORM) [13] is based on the linearization of the failure surface at the "design point", or the most likely point of failure. Each component of the parameter vector $\boldsymbol{\theta}$ is transformed such that $\widehat{\boldsymbol{\theta}} = \widehat{T}(\boldsymbol{\theta})$ is in standard normal space. The performance function is transformed as well, so that $\widehat{g}(\widehat{\boldsymbol{\theta}}) = g(\widehat{T}(\boldsymbol{\theta}))$. The design point is defined as the point $\widehat{\boldsymbol{\theta}}^*$ on the failure surface that lies closest to the origin. The failure surface is then approximated as a plane passing through this design point, and the failure probability is given by $p_f = \Phi(-\widehat{\beta})$ where $\widehat{\beta} = \|\widehat{\boldsymbol{\theta}}^*\|$ and Φ is the standard normal *cumulative distribution function* (c.d.f.). For many problems, particularly those with relatively few input parameters and an approximately linear failure surface, FORM is the most efficient method for calculating the failure probability. But finding the design point becomes expensive if there are a large number of parameters. Also, it is not possible to estimate the accuracy of the result without employing an additional method such as MCS.

Line sampling [14, 34] is a variance reduction technique, meaning it is designed so that the coefficient of variation (CoV), δ_{LS}, of the resulting estimator $\bar{p}_f$ is smaller than δ_{MC}. The key idea behind line sampling is to reduce the dimension of the problem, and let the failure surface be a function of $d-1$ parameters, so that one parameter, $\theta_1 = g_{-1}(\boldsymbol{\theta}_{-1})$, is on the failure surface and the reduced parameter set is $\boldsymbol{\theta}_{-1} = \{\theta_2, ..., \theta_d\}$. Like FORM, line sampling requires that $\boldsymbol{\theta}$ be transformed into standard normal space, and the normalized joint probability density function is given by

$$\widehat{h}(\widehat{\boldsymbol{\theta}}) = \prod_{i=1}^{d} \phi(\widehat{\theta}_i)\,.$$

The quantity $\widehat{\theta}_1 = \widehat{g}_{-1}(\widehat{\boldsymbol{\theta}}_{-1})$ is the height of the failure surface at $\widehat{\boldsymbol{\theta}}_{-1}$ in the rotated

coordinate system $(\widehat{\boldsymbol{\theta}}_{-1}, \widehat{\theta}_1)$. It can be shown that (see [14]) the probability of failure is equal to the expectation of the random variable $\Phi(\widehat{g}_{-1}(\widehat{\boldsymbol{\theta}}_{-1}))$. A Monte Carlo estimate of p_f is

$$\bar{p}_f = \frac{1}{N} \sum_{i=1}^{N} \Phi\left(\widehat{g}_{-1}\left(\widehat{\boldsymbol{\theta}}_{-1}^{(i)}\right)\right). \tag{6}$$

where Φ is the standard normal cumulative distribution function. Unlike FORM, it is possible to analytically estimate the accuracy of the $\bar{p}_f$ computed using line sampling. The variance of the estimator is given by:

$$\mathrm{Var}\left[\bar{p}_f\right] = \frac{1}{N}\mathrm{Var}\left[\Phi\left(\widehat{g}_{-1}\right)\right]. \tag{7}$$

While the CoV of the line sampling estimator, δ_{LS} depends on the choice of search direction $\widehat{\theta}_1$, it is always less than or equal to δ_{MC}.

Subset simulation [15] is another variance reduction technique, but rather than dimensional reduction, it employs *conditional probability* to reduce the variance of the estimator for p_f. Subset simulation is based on the fact that the probability of a rare failure event can be expressed as the product of the probabilities of more frequent intermediate events. For example, given a failure event F, let $F_1 \subset F_2 \subset \ldots \subset F_m = F$ be a decreasing sequence of failure events. Using the definition of conditional probability, the probability of failure is given by:

$$p_f = P\left(F_m\right) = P\left(\bigcap_{i=1}^{m} F_i\right) = P\left(F_1\right) \prod_{i=1}^{m-1} P\left(F_i | F_{i-1}\right). \tag{8}$$

The key to the implementation of subset simulation is the ability to generate samples according to the conditional distribution of $\boldsymbol{\theta}$ given that it lies in F_i. Markov chain Monte Carlo simulation is an efficient method for generating samples according to an arbitrary distribution, and in this case, a modified Metropolis algorithm is used to generate a Markov chain with the stationary distribution $q(\cdot|F_i)$.

This algorithm is described in Appendix A. As with line sampling, the coefficient of variation of the estimator generated by subset simulation can be calculated directly, and the details of this calculation can be found in [15].

4. Results

In the previous section we have seen that MCS is expensive if the desired p_f is small. Hundreds, or even thousands, of Monte Carlo simulations may be needed before we can be confident that a structure will not fail at given load. This is the primary reason for the lack of penetration of reliability analysis in the routine design of sandwich composite structures. We have also examined a few methods that have been developed in recent years with the aim of reducing the number of simulations needed. Can these advanced techniques be employed to reduce the number of simulations needed for an accurate analysis of the reliability of sandwich composites? The results in this section suggest that, in general, the answer is no.

To evaluate the performance of each technique, the probability of failure of a sandwich composite with an insert was computed over a range of applied loads, and calculated failure probabilities, coefficients of variation, and iteration counts for the four techniques were then compared for each load. Two methods of determining global failure were examined, two-component failure and three-component failure, as discussed in Section 2.3.

4.1. Input statistics and sensitivity

The sandwich panel geometry and material properties were obtained from [10]. The input parameter vector, $\boldsymbol{\theta}$, consisted of 19 parameters describing the geometry, stiffnesses, and failure stresses. The geometric parameters were r_a, r_c, r_p,

Table 1: Mean values of the parameters that compose the vector $\boldsymbol{\theta}$.

Geometry		**Stiffness**		**Failure Stress**	
r_a	40 mm	C_{11}^{face}	110 GPa	σ_y^{pot}	40 MPa
r_c	35 mm	C_{12}^{face}	53 GPa	σ_f^{core}	14 MPa
r_p	15 mm	C_{22}^{face}	53 GPa	τ_f^{core}	0.18 MPa
r_i	5 mm	C_{33}^{core}	2.2 GPa	σ_t^{face}	400 MPa
f	0.5 mm	C_{55}^{core}	610 MPa	σ_c^{face}	400 MPa
c	19 mm	C_{33}^{pot}	3.4 GPa	σ_b^{face}	400 MPa
		C_{55}^{pot}	1.9 GPa		

r_i, f, and c (see Figure 2); the stiffness parameters were C_{11}^{face}, C_{12}^{face}, C_{22}^{face}, C_{33}^{core}, C_{55}^{core}, C_{33}^{pot}, and C_{55}^{pot}; and the failure stress parameters were the yield stress of the potting (σ_y^{pot}), the normal and shear failure stresses in the core ($\sigma_f^{\text{core}}, \tau_f^{\text{core}}$), the uniaxial tensile and compressive failure stresses ($\sigma_t^{\text{face}}, \sigma_c^{\text{face}}$) and the biaxial tensile failure stress (σ_b^{face}) in the facesheets.

Each parameter was assigned a Gaussian distribution with mean values given in Table 1. The CoVs were 0.01 for r_a, r_c, f, c; 0.1 for r_p; 0.02 for r_i; 0.1 for the potting stiffness; 0.01 for the facesheet stiffness; 0.2 for the core stiffness; 0.1 for the potting and core failure stress; and 0.05 for the facesheet failure stress. Note that these estimates of variability are probably more appropriate for fiber-reinforced polymer/Nomex honeycomb core sandwich composites than for aluminum-aluminum sandwich panels.

The assumed values of the CoVs are worth examination. In most marine and aerospace sandwich structures, the thicknesses of the facesheet and the core are tightly controlled and a global variability of 1-2% is observed. Our simulations

model a standard insert pull-out test for which the radius of the panel and the radius of the clamped region are also tightly specified. There is less control over the radius of the insert, but the variability can still be assumed to be quite small. However, the effective radius of the adhesive potting can change dramatically depending on the location of the insert relative to the honeycomb geometry; a 10-20% difference between two samples is quite routine. The facesheet stiffness varies little between samples, especially if the facesheet is thin. On the other hand, we have found that the core stiffness can be significantly different from sample to sample because it depends strongly on the geometry of the honeycomb. This is even more so when we consider foam cores. The stiffness of the potting is affected by the presence of voids. The 10% variability that we have assumed attempts to take the effect of gas pockets into account. The variability in the failure stress of the potting does not take voids into consideration and hence is lower than that for the potting stiffness. The core failure stress is dominated by localized buckling and tensile failure and the variation is less than that of the core stiffness, which is a global quantity. The variation in the facesheet failure stress is usually quite small for thin facesheets. However, larger CoVs should be used for thick facesheets.

It is implicit in the above that the parameters are independent. However, there is a correlation between the geometry of the honeycomb and its stiffness and strength properties. Simplified models, such as those discussed in [32], can be used to reduce the number of independent variables. The resulting expressions, though exact, can be quite involved. If enough experimental data is available on the distributions of the parameters, correlations may be computed and the vector $\boldsymbol{\theta}$ can be transformed into an independent set using classical transformations.

A sensitivity analysis can also be used to reduce the length of the vector $\boldsymbol{\theta}$. We

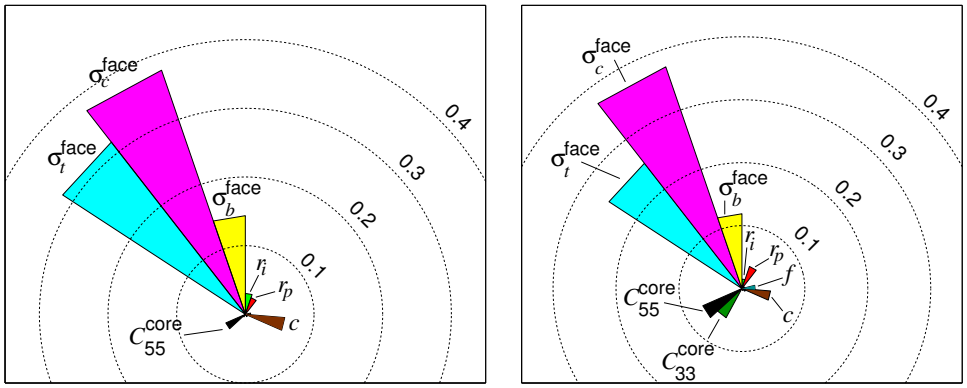

Figure 5: Rosette plots showing the sensitivity of global failure to the input parameters at a load where the probability of failure is ∼50%. The plot on left is for two-component failure and that on the right is for three-component failure. Only parameters with a sensitivity index greater than 0.01 are labelled.

have not used sensitivity information for the reliability calculations in this work. However, for completeness, we have calculated, using Sobol's Method [35], the total global sensitivity indices for each of the input variables. In order to best identify the factors that determine structural failure, these analyses were carried out at loads where the probability of failure is near 50%: 3.25 kN for the two-component failure model and 3.55 kN for the three-component failure model. The rosette plots in Figure 5 indicate which of the input parameters have the largest impact for the two- and three-component cases. Our calculations with the Thomsen model suggest that the critical mode in both cases is the failure of one or both facesheets and it is not surprising that the most critical parameters are the facesheet failure strengths. The parameters that govern the shear stiffness of the core, C_{55}^{core} and c play a large role as well, as these determine how much of the pullout load must be carried by the facesheets.

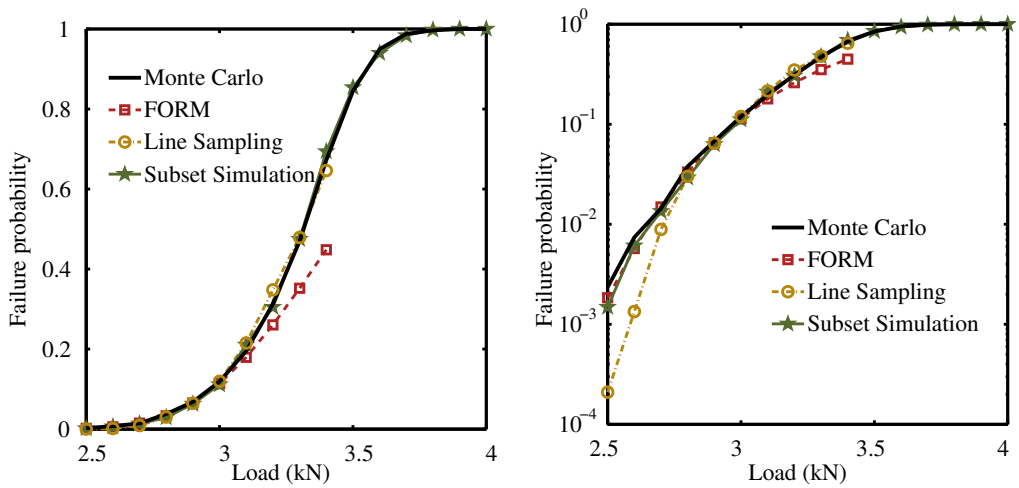

Figure 6: Failure probabilities calculated by MCS, subset simulation, line sampling, and FORM for the situation where global failure requires that at least two components fail.

4.2. Reliability: Two-component failure

For the "two-component failure" case, we find that the structure has the possibility of failure at loads greater than 2.5 kN; and it is guaranteed to fail at loads greater than 4 kN. Figure 6 shows the failure probabilities at each load, on both a linear and a log scale. Note that the failure loads are considerably lower than the $\sim$5 kN observed in experiments. The discrepancy is partly due to the excessively stiff response of the panel because geometric nonlinearities and localized material nonlinearities have not be taken into account. We will not pursue these reasons further in this paper because they involve the accuracy of the model rather than the accuracy of the reliability calculations. As shown in Figure 6, both the subset simulation and FORM results agree well with MCS for low ($<$1%) failure probabilities, but only subset simulation provides an accurate estimate of p_f over the entire range of applied loads. Line sampling severely underestimates the probability of failure at low loads, and FORM did not converge for loads above 3.4

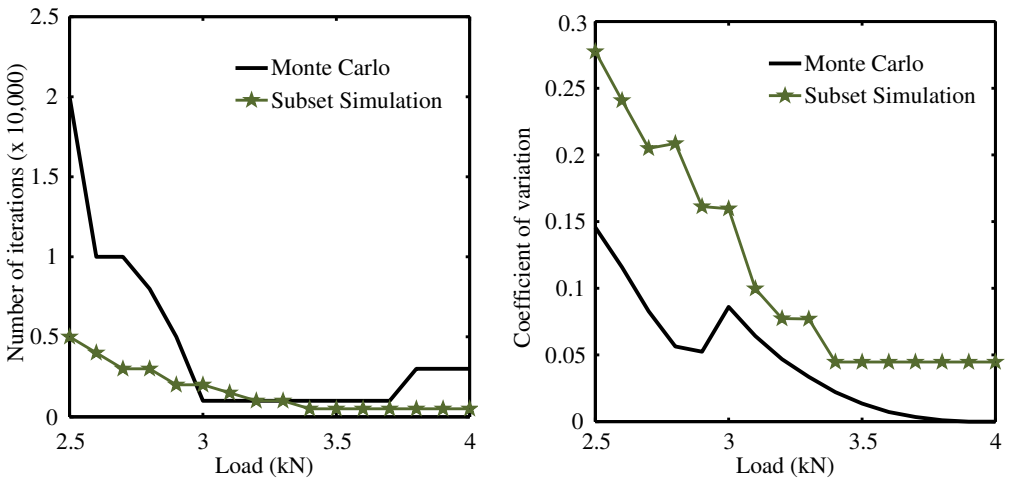

Figure 7: Number of simulations and coefficient of variations for MCS and subset simulation for two-component failure.

kN.

The shape of the failure surface is responsible for the poor results generated by line sampling and FORM. In our model the core always fails first. But the second component to fail can be either the top or bottom face sheet, depending on the input parameters. The FORM fails to converge at high loads because the optimization algorithm fails to deal with a ridge in the performance function due to the transition from one failure mode to the other. Similarly, at low loads, the line sampling algorithm appears to capture only a single mode of failure, and therefore overestimates the reliability of the structure. Because subset simulation does not rely on a directional vector in parameter space or an optimisation procedure, it is unaffected by the shape of the failure surface. However, as shown in Figure 7, *while the number of subset simulation iterations is lower than the number Monte Carlo iterations, the computed CoVs show that MCS is more accurate.*

Because both the number of simulations and the CoVs for the two methods vary,

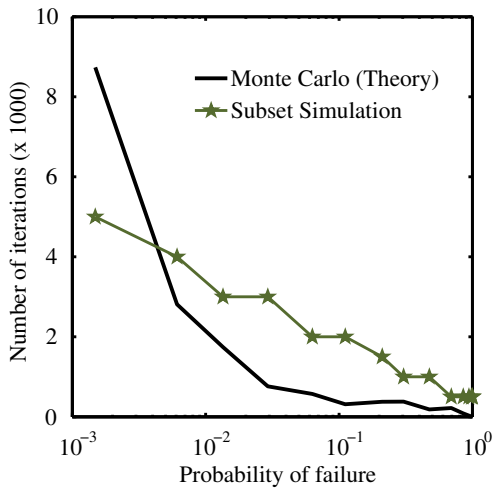

Figure 8: Comparison of the efficiencies of subset sampling and Monte Carlo for two-component failure.

it is difficult to directly compare their efficiency. However, this can be addressed by calculating the number of Monte Carlo samples necessary to generate the CoV associated with subset simulation for each load case:

$$N_t = \frac{1 - p_f}{p_f \delta_{\mathrm{SS}}^2}.$$

Here, δ_{SS} is the CoV of the subset simulation estimate. Figure 8 shows the number of iterations performed in each subset simulation analysis as well as the number of Monte Carlo samples that would be required to achieve the same CoV. This clearly shows that *MCS would be more efficient* in all cases where the probability of failure was greater than 5×10^{-3}.

4.3. Reliability: Three-component failure

The second reliability analysis considers the situation where global failure of the sandwich panel occurs when at least *three* of the constituent components have met their failure criteria. Using this definition of failure, the relevant range of

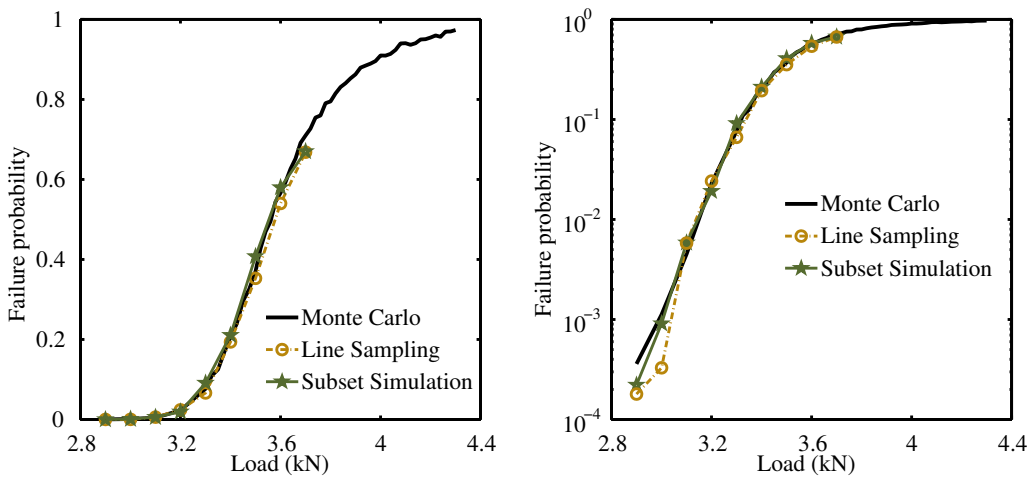

Figure 9: Failure probabilities calculated by MCS, subset simulation, line sampling, and FORM for three-component failure.

failure loads was found to be from 2.9 kN to 4.3 kN. The failure probabilities in this range are shown in Figure 9. Because it was established in Section 4.3 that MCS is the most efficient method for high failure probabilities, subset simulation and line sampling were not performed for loads greater than 3.7 kN. In addition, no results are given for FORM because the method did not converge to a solution at the relevant loads. In this case, the line sampling algorithm deals with the shape of the failure surface more effectively and is reasonably accurate even for low failure probabilities.

The number of iterations and coefficients of variation for three-component failure are given in Figure 10. As in the prior case, MCS requires the greatest number of iterations, but also provides the most accurate estimate. Subset simulation is once again much more accurate than line sampling at low loads.

Using the technique described in Section 4.3, the required MCS iteration count was calculated for comparison with the subset simulation analysis. As shown

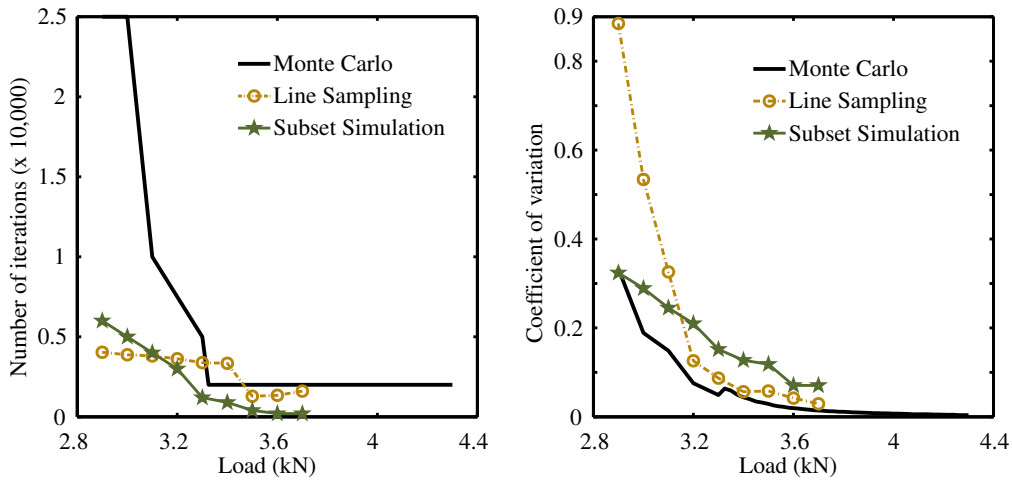

Figure 10: Number of simulations and coefficient of variations for MCS and subset simulation for three-component failure.

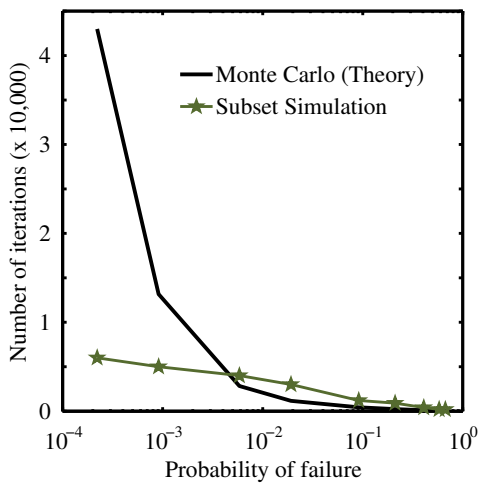

Figure 11: Comparison of the efficiencies of subset sampling and Monte Carlo for three-component failure.

in Figure 11, MCS again outperforms the variance reduction method for failure probabilities above about 5×10^{-3}. However, for much lower failure probabilities, subset simulation reduces the number of required iterations by approximately nine times.

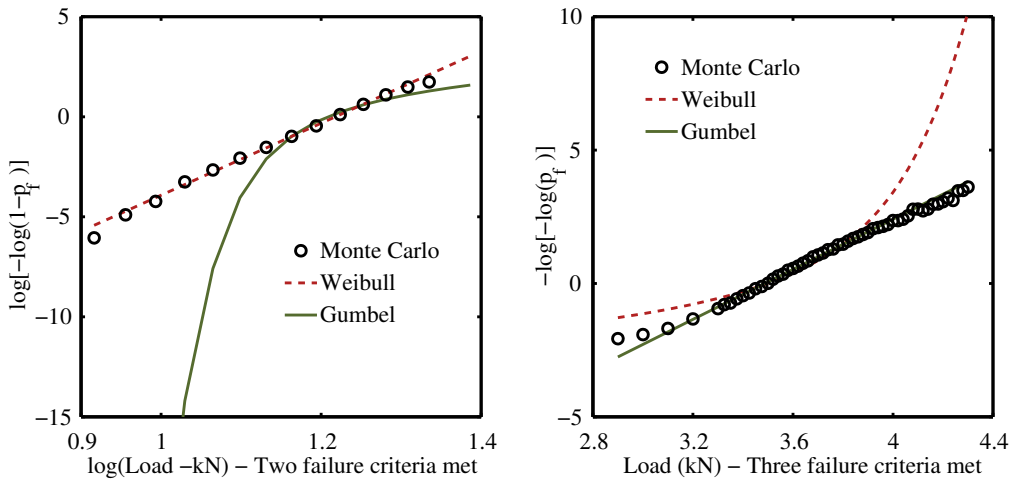

Figure 12: Two- and three-component failure models compared with the Weibull and Gumbel distributions, respectively, in transformed space.

4.4. Failure Probability Distribution

To better understand the results of the reliability analyses, the failure probability curves were compared to a variety of distributions, including the normal, lognormal, Weibull, and Gumbel distributions. The normal and lognormal distributions did not fit either reliability analysis, but the two-component failure model fit a Weibull distribution, and the three-component model fit a Gumbel distribution as can be seen in Figure 12. In order to make the distinction between the two distributions obvious the results have been plotted in transformed space so that the simulated data lie approximately on a straight line. The fitted equations and the coordinate transformations are given in Appendix B. Using the fitted distribution, the average load for two-component failure is $\sim$3.3 kN with a standard deviation of $\sim$0.2 kN; for three component failure the load is $\sim$3.6 kN with a standard deviation of $\sim$0.3 kN.

In our model, the probability of overall structural failure is determined primar-

ily by facesheet failure, due to the fact that the core and the potting fail at very low and very high loads, respectively. Therefore, in the two component case, structural failure occurs when at least one facesheet fails (the minimum of the two criteria), and in the three component case, failure occurs when both facesheets fail (the maximum). Because a stress based reliability analysis captures the maximum values of the failure criteria within each component, the distribution of failure loads is typically described by an extreme value distribution. The Weibull distribution describes the distribution of the minimum of a set of extreme values, and the Gumbel distribution describes the maximum of a set of extreme values, so the results given above are reasonable.

5. Discussion and Conclusions

This study has shown that in certain circumstances, variance reduction methods may be useful for reducing the amount of computational effort required for the reliability analysis of a composite sandwich structure. When the probability of failure is anticipated to be below about 0.1%, subset simulation provides a significant reduction in the number of required structural evaluations while maintaining the flexibility associated with MCS. Line sampling and FORM are not as effective for problems in composites due to the fact that they do not deal effectively with multiple failure modes. There are some special situations, particularly for non-critical inserts in marine composites, where relatively large failure probabilities in the range of 0.5% to 5% are acceptable. This study has shown that none of the available reliability analysis techniques can improve upon MCS in this range. For lower failure probabilities, though subset simulation provides a stable and more efficient alternative, the required number of simulations continues to be in

the thousands. The implication of this result is that accurate characterisation of the reliability of composite structures will require either parallel computers capable of carrying out thousands of detailed simulations in a short period of time or the development of reduced-order models that capture the important facets of the behavior of the structure.

Acknowledgment

This work has been supported by The Foundation for Research Science and Technology of New Zealand through Grant UOAX0710 and Altitude Aerospace Interiors. We would also like to thank Dr. Emilio Calius, Dr. Mark Battley, and Dr. Temoana Southward for introducing us to the problem. Thanks are also due to an anonymous reviewer for pointing out inconsistencies and helping improve the paper.

Glossary

p_f	probability of failure
CoV	coefficient of variation
r_i	radius of insert
r_p	radius of potting
r_c	radius of clamped region
r_a	radius of panel
$2c$	core thickness
$2f$	facesheet thickness
C_{ij}	elastic stiffness of facesheet
C_{33}	elastic transverse stiffness of core/potting

C_{33}	elastic shear stiffness of core/potting
S_{55}	elastic shear compliance of core/potting
A_{ij}	extensional stiffness of facesheet
D_{ij}	bending stiffness of facesheet
σ_{rr}	radial stress
$\sigma_{\theta\theta}$	circumferential stress
σ_{rz}	transverse shear stress
σ_{zz}	transverse normal stress
ε_{rr}	radial strain
$\varepsilon_{\theta\theta}$	circumferential strain
ε_{rz}	transverse shear strain
Ω_0	reference surface of facesheet
Γ_0	boundary of reference surface
N_{rr}	radial stress resultant
$N_{\theta\theta}$	circumferential stress resultant
u_{0r}	radial displacement
s	external shear traction
N_r	external normal force on Γ_0
M_r	external moment on Γ_0
Q_z	external shear force on Γ_0
M_{rr}	radial stress moment resultant
$M_{\theta\theta}$	circumferential stress moment resultant
w_0	out-of-plane displacement
$\boldsymbol{\theta}$	vector of uncertain parameters
$\widehat{\boldsymbol{\theta}}$	normalized vector of uncertain parameters

$g(\boldsymbol{\theta})$	performance function
$h(\boldsymbol{\theta})$	joint probability density function
F	failure event
σ_y	yield stress
σ_f	normal stress at failure
τ_f	shear stress at failure
σ_t	uniaxial tensile stress at failure
σ_c	uniaxial compressive stress at failure
σ_c	biaxial tensile stress at failure
Φ	standard normal cumulative distribution function
ϕ	standard normal probability density function

References

[1] S. Heimbs, M. Pein, Failure behaviour of honeycomb sandwich corner joints and inserts, Composite Structures 89 (4) (2009) 575–588.

[2] N. Raghu, M. Battley, T. Southward, Strength variability of inserts in sandwich panels, in: Proc. , Eighth International Conference on Sandwich Structures, Porto, 2008, pp. 558–569.

[3] P. Bunyawanichakul, B. Castanie, J.-J. Barrau, Experimental and numerical analysis of inserts in sandwich structures, Applied Composite Materials 12 (2005) 177–191.

[4] M. A. Roth, Development of new reinforced load introductions for sandwich structures, in: O. T. Thomsen, E. Bozhevolnaya, A. Lyckegaard (Eds.), Sandwich Structures 7: Advancing with Sandwich Structures and Materials, Spirnger, Dordrecht, 2005, pp. 987–996.

[5] E. V. Iarve, R. Kim, D. Mollenhauer, Three-dimensional stress analysis and Weibull statistics based strength prediction in open hole composites, Composites Part A: Applied Science and Manufacturing 38 (1) (2007) 174–185.

[6] E. V. Iarve, D. Mollenhauer, T. J. Whitney, R. Kim, Strength prediction in composites with stress concentrations: Classical Weibull and critical failure volume methods with micromechanical considerations, Journal of Materials Science 41 (20) (2006) 6610–6621.

[7] S. Sihn, E. V. Iarve, A. K. Roy, Asymptotic analysis of laminated composites with countersunk open- and fastened-holes, Composites Science and Technology 66 (14) (2006) 2479–2490.

[8] K.-I. Song, J.-Y. Choi, J.-H. Kweon, J.-H. Choi, K.-S. Kim, An experimental study of the insert joint strength of composite sandwich structures, Composite Structures 86 (2008) 107–113.

[9] N. Raghu, M. Battley, T. Southward, Strength variability of inserts in sandwich panels, Journal of Sandwich Structures and Materials 11 (6) (2009) 501.

[10] G. Bianchi, G. S. Aglietti, G. Richardson, Static Performance of Hot Bonded and Cold Bonded Inserts in Honeycomb Panels, Journal of Sandwich Structures and Materials (2010) doi:10.1177/1099636209359840.

[11] O. T. Thomsen, W. Rits, Analysis and design of sandwich plates with inserts - a higher order sandwich plate theory, Composites Part B 29B (1998) 795–807.

[12] J. C. Helton, J. D. Johnson, W. L. Oberkampf, Verification of the calculation of probability of loss of assured safety in temperature-dependent systems with multiple weak and strong links, Reliability Engineering and System Safety 92 (10) (2007) 1363–1373.

[13] A. M. Hasofer, N. C. Lind, Exact and invariant second-moment code format, ASCE J. Eng. Mech. 100 (EM 1) (1974) 111–121.

[14] P. S. Koutsourelakis, H. J. Pradlwarter, G. I. Schueller, Reliability of structures in high dimensions, Part I: Algorithms and applications, Probabilistic Engineering Mechanics 19 (4) (2004) 409–417.

[15] S. K. Au, J. L. Beck, Estimation of small failure probabilities in high dimensions by subset simulation, Probabilistic Engineering Mechanics 16 (4) (2001) 263–277.

[16] F. J. Plantema, Sandwich Construction, John Wiley and Sons, New York, 1966.

[17] W. S. Burton, A. K. Noor, Assessment of continuum models for sandwich panel honeycomb cores, Comput. Methods Apl. Mech. Engrg. 145 (1997) 341–360.

[18] L. Vu-Quoc, I. K. Ebcioğlu, H. Deng, Dynamic formulation for geometrically-exact sandwich shells, Int. J. Solids Struct. 34 (20) (1997) 2517–2548.

[19] T. Anderson, E. Madenci, W. S. Burton, J. Fish, Analytical solution of finite-geometry composite panels under transient surface loading, Int. J. Solids Struct. 35 (12) (1998) 1219–1239.

[20] A. Barut, E. Madenci, J. Heinrich, A. Tessler, Analysis of thick sandwich construction by a {3,2}-order theory, Int. J. Solids Struct. 38 (2001) 6063–6077.

[21] A. Barut, E. Madenci, T. Anderson, A. Tessler, Equivalent single-layer theory for a complete stress field in sandwich panels under arbitrary distributed loading, Composite Structures 58 (2002) 483–495.

[22] L. Vu-Quoc, I. K. Ebcioğlu, General multilayer geometrically-exact beams/1-d plates with deformable layer thickness: Equations of motion, Z. Angew. Math. Mech. 80 (2000) 113–136.

[23] Y. Frostig, O. T. Thomsen, I. Sheinman, On the non-linear high-order theory of unidirectional sandwich panels with a transversely flexible core, Int. J. Solids Struct. 42 (2005) 1443–1463.

[24] R. A. Arciniega, J. N. Reddy, Large deformation analysis of functionally graded shells, Int. J. Solids Struct. 44 (2007) 2036–2052.

[25] R. A. Arciniega, J. N. Reddy, Tensor-based finite element formulation for geometrically nonlinear analysis of shell structures, Comput. Methods Appl. Mech. Engrg. 196 (2007) 1048–1073.

[26] J. Hohe, L. Librescu, Recent results on the effect of the transverse core compressibility on the static and dynamic response of sandwich structures, Composites: Part B 39 (2008) 108–119.

[27] O. T. Thomsen, Sandwich plates with 'through-the-thickness' and 'fully potted' inserts: evaluation of differences in structural performance, Composites Structures 40 (2) (1998) 159–174.

[28] O. T. Thomsen, High-order theory for the analysis of multi-layer plate assemblies and its application for the analysis of sandwich panels with terminating plies, Composites Structures 50 (2000) 227–238.

[29] O. Rabinovitch, Y. Frostig, High-order behavior of fully bonded and delaminated circular sandwich plates with laminated face sheets and a "soft" core, Int. J. Solids Struct. 39 (2002) 3057–3077.

[30] G. M. Kulikov, E. Carrera, Finite deformation higher-order shell models and rigid-body motions, Int. J. Solids Struct. 45 (2008) 3153–3172.

[31] B. Banerjee, B. Smith, The Thomsen model of inserts in sandwich composites: An evaluation, arXiv:cond-mat 1009.5431v1 (2010) 1–30.

[32] L. Gibson, M. Ashby, Cellular solids: structure and properties, Cambridge Univ Pr, 1999.

[33] D. Mohr, M. Doyoyo, Deformation-induced folding systems in thin-walled monolithic hexagonal metallic honeycomb, International journal of solids and structures 41 (11-12) (2004) 3353–3377.

[34] G. I. Schueller, H. J. Pradlwarter, P. S. Koutsourelakis, A critical appraisal of reliability estimation procedures for high dimensions, Probabilistic Engineering Mechanics 19 (4) (2004) 463–474.

[35] I. Sobol', Sensitivity estimates for nonlinear mathematical models, MMCE 1 (4) (1993) 407–414.

Appendix A. Subset simulation implementation details

Appendix A.1. Markov Chain Monte Carlo

The key to the implementation of subset simulation is the ability to generate samples according to the conditional distribution of $\boldsymbol{\theta}$ given that it lies in F_i: $q(\boldsymbol{\theta}|F_i) = q(\boldsymbol{\theta})\mathbf{1}_{F_i}(\boldsymbol{\theta})/P(F_i)$. Markov-chain Monte Carlo simulation is an efficient method for generating samples according to an arbitrary distribution. In our work, a modified Metropolis algorithm is used to generate a Markov chain with the stationary distribution $q(\cdot|F_i)$. The modified Metropolis algorithm is a two step process for generating additional samples, and relies on a "proposal PDF", $p_j^*(\xi_j|\theta_j)$ for generating samples around each component of $\boldsymbol{\theta}$. The proposal PDF is a one dimensional PDF centered at θ_j with the symmetry property $p_j^*(\xi_j|\theta_j) = p_j^*(\theta_j|\xi_j)$. In this study, p_j^* is chosen as the uniform distribution with a width of one standard deviation.

Appendix A.2. Intermediate Failure Events

The second key implementation detail is the choice of the intermediate failure events $F_1, ..., F_{m-1}$. While it is possible to choose the conditional failure values g_i *a priori*, the implementation of the method is more straightforward if the g_i are chosen adaptively so that the conditional probabilities are equal to a fixed value p_0. This is accomplished by choosing g_i as the $(1 - p_0)N$th largest value from $g(\boldsymbol{\theta}_i^{(k)}) : k = 1, ..., N$. The conditional probability p_0 is chosen to reflect a balance between the number of required conditional levels and the number of

samples per level. Here, a value of 0.2 has been chosen for low loads, and 0.5 has been used at higher loads.

Appendix B. Weibull and Gumbel distributions and transformations

The distributions fitted to the results of the Monte Carlo simulations of the two- and three-component failure models (see Figure 12) were:

$$p_f(x) \approx 1 - e^{-(x/\lambda)^k} \quad = 1 - e^{-(x/3380)^{18}} \qquad \text{Two-component failure,}$$

$$p_f(x) \approx e^{-e^{-(x-\mu)/\beta}} \quad = e^{-e^{-(x-3490)/209}} \qquad \text{Three-component failure.}$$

The Weibull distribution is defined by the cumulative distribution function:

$$p_w(x) = 1 - e^{-(x/\lambda)^k}.$$

Let the transformation T_w be defined as $T_w(f) = \log[-\log(1-f)]$, and let $\tilde{x} = \log x$. Applying T_w to $p_w(\tilde{x})$ gives:

$$T_w[p_w(\tilde{x}]) = \log\left[-\log\left(e^{-(\exp\tilde{x}/\lambda)^k}\right)\right] = k\tilde{x} - k\log\lambda,$$

so a plot of $\tilde{x} = \log x$ versus $T_w(p_w)$ is a straight line. Similarly, the Gumbel distribution is defined by the c.d.f:

$$p_g(x) = e^{-e^{-\frac{x-\mu}{\beta}}}.$$

Applying the transformation $T_g(f) = -\log(-\log f)$ to p_g gives:

$$T_g[p_g(x)] = -\log\left[-\log\left(e^{e^{-(x-\mu)/\beta}}\right)\right] = \frac{1}{\beta}x - \frac{\mu}{\beta},$$

so x versus $T_g(p_g(x))$ is a line. The transformations T_w and T_g were used to create the plots shown in Figure 12.